

**The Influence of Volatile Loss During the
Emplacement of Lava Flows**

Stephen M. Baloga¹
Lori S. Glaze¹
Matthew N. Peitersen¹
Joy A. Crisp²

Submitted to Jour. Geophys. Research
March 27, 1999

¹ Proxemy Research
20528 Farcroft Lane
Laytonsville, MD 20882

² Jet Propulsion Laboratory
California Institute of Technology
Pasadena, California

ABSTRACT

The density of lava that formed some recent Hawaiian basaltic lava flows changed over the course of the eruption and changed with distance from the vent. We present a theoretical model of a lava flow that continuously loses volatiles during flow advance and has a bulk viscosity that is a function of distance from the vent. Governing equations for the flow thickness and the bulk density profiles are derived by considering mass and volume conservation. Because the mass loss associated with degassing is negligible, the loss of volatiles results in a change in density along the flow path.

Our generic formulation can accommodate different types of flow rates and models of volatile loss during emplacement. We consider two endmember flow rates, Newtonian and Basal Glide, with cubic and linear dependences on flow thickness, respectively. We also consider two

types of volatile loss rates, one that is constant and another that depends on the thickness of the flow. Linear and exponential models for the change in rheology with distance are investigated with the combinations above. The model is constructed so that field estimates can be used to obtain the necessary parameters in lieu of more detailed experimental or theoretical studies of degassing in active flows. Formulas are tabulated for thickness and density profiles for various combinations of flow rates, rheologic changes, and degassing rate functions. We also tabulate formulas for estimating parameters associated with the form and rate of degassing from field data.

Examples of thickness and density profiles are given for a flow with a length, thickness, underlying slope, and emplacement time comparable to the main "1 Flow" from the 1984 eruption of Mauna Loa. These profiles are computed for a range of lava densities reported for this eruption. We also investigate the influence of the two different rate functions for the loss of volatiles during emplacement and the two models of viscosity changes.

A bulk density increase due to degassing during emplacement may have a significant influence on the thickness of a lava flow and the rate at which it advances. For relatively high rates of degassing, the flow profile has a maximum thickness located progressively closer to the vent as the rate of degassing increases. Degassing while a flow is active increases the duration of emplacement by as much as 60% for flows with dimensions and parameters like those of the recent Mauna Loa flow. Thus, the parameters that define the rate of degassing, and the consequent density change along the path of a flow, emerge as important variables for a quantitative understanding of flow emplacement.

The Influence of Volatile Loss During the Emplacement of Lava Flows

1. INTRODUCTION

The density of lava that formed some recent Hawaiian basaltic lava flows was reported to change over the course of the eruption and change with distance from the vent [Moore, 1982, 1987; Lipman and Banks, 1987]. Data from the 1984 eruption of Mauna Loa clearly indicates significant changes occurred during the eruption and emplacement of lava flows. The bulk lava density at the vent appears to have gradually decreased in time, while density in the primary flow lobe increased with distance from the vent. Moore [1982, 1987] inferred differences between erupted and emplaced volumes of lava flows from the 1942 and 1984 eruptions of Mauna Loa which he attributed to significant density increases during emplacement. These and other studies [e.g. Einarsson et al., 1949; Cashman et al., 1994] suggest that differences between erupted and emplaced volumes of lava may be quite common in basaltic and basaltic andesite flows. Malin [1980] mentioned that post-emplacement deflation of Hawaiian flows could result in volume losses, and hence under-estimations of effusion rates, approaching 50%. Hon et al. [1994] noted the presence of both inflation and deflation in pahoehoe sheet flows, although they primarily investigated inflation.

These field observations suggest that volume losses during emplacement can cause an increase in the bulk density as the lava flow advances. When this occurs, volume conservation must be considered in conjunction with the conservation of mass to account for both volatile losses and

changes in the lava density. In active flows, the degassing process does not occur in isolation. Changes in viscosity, eruption conditions, temperature, crystal content, pre-existing topography, and losses to stationary components of the flow all compete to some extent with the processes that influence how lava volume is conserved. In this work, we focus only on the combined effects of viscosity and density changes along the flow path.

The governing equations for the flow thickness and density profiles are derived below by considering mass and volume conservation. To illustrate the mathematical derivations, we highlight a Newtonian flow rate. We briefly consider an alternative volume flow rate that features a linear dependence on the flow depth. We also consider two types of volatile loss rates, one that is constant and another that depends on the thickness of the flow. Linear and exponential models for the change in rheology with distance are investigated with the combinations above. Formulas are tabulated for thickness and density profiles for various combinations of flow rates, rheologic changes, and degassing rate functions. We also tabulate formulas for estimating parameters associated with the form and rate of degassing from field data.

The lava flow degassing model we develop in this work is constructed so that field estimates can be used to obtain the necessary parameters in lieu of more detailed experimental or theoretical studies. The degassing of magmas in conduits and magma chambers, and its effect on eruption mechanisms, has been dealt with extensively in the literature [cf. Wadge, 1981; Wilson and Head, 1981; Taylor et al., 1984; Westrich et al., 1988]. Surface degassing in ponds and lava fountains has also been considered [cf. Sparks and Pinkerton, 1978; Wallace and Anderson, 1998].

The effect of degassing during flow emplacement has received less attention. Sparks and Pinkerton [1978] noted fundamental changes in rheology following degassing in fire fountains. They suggested that downflow changes in the rheology of lava flows might be caused by crystallization due to this gas loss. Although degassing mechanisms (bubble formation, growth, and coalescence) have been explored in detail [cf. Sparks, 1978; Prousevitch et al., 1993; Cashman et al., 1994], none of these studies provides sufficient data to determine the rate of volatile loss from a parcel of lava during the emplacement of an active flow.

We present steady-state thickness and density profiles for a flow that has a length, thickness, underlying slope, and emplacement time comparable to the 1 Flow from the 1984 eruption of Mauna Loa. Different scenarios for the loss of volatiles and viscosity changes are considered. Although the detailed nature of degassing of the 1 Flow is not known, we consider a range of plausible densities that are consistent with the available field measurements.

We conclude that degassing during emplacement can have a significant influence on the thickness of a lava flow and the emplacement time. Thus, the parameters that define the rate of degassing, and the consequent density change along the path of a flow, emerge as important variables for a quantitative understanding of flow emplacement.

2. THE MODEL

Governing Equations

We begin the derivation of governing equations by considering lava mass and volume conservation expressions for a control volume of thickness h , width w , and length dx at an arbitrary point along the flow path. The mass of gas lost from the control volume is negligible compared to the mass of lava in the control volume. Consequently, we can write the mass conservation as

$$\frac{\partial}{\partial t}(\rho h) + \frac{\partial}{\partial x}(\rho q) = 0 \quad (1)$$

where $\rho(x,t)$ is the density of the lava and q is the volume flow rate. (See Table 1 for definitions of the mathematical symbols used in this paper). This equation simply indicates that any gradient in the mass flux through the control volume must be compensated by a change in the mass of the control volume with time.

The volume of gas lost from the degassing control volume is *not* negligible if it causes a density change. Thus, the volume conservation expression must have a loss on the right hand side of the expression

$$\frac{\partial}{\partial t}(h) + \frac{\partial}{\partial x}(q) = -\lambda h_o \Phi(h,x,t) \quad (2)$$

where Φ is a dimensionless function that describes how volatiles are lost and λ is a conventional rate constant. The length scale for the degassing process on the right side of (2) is taken, for convenience, as the initial flow thickness at the vent. Both (1) and (2) implicitly assume a constant flow width

by using q , the volume flow rate per unit width. However, solutions for a variable width can also be determined by following the approach outlined below.

By expanding (1) and using (2), one finds

$$h \frac{\partial \rho}{\partial t} + q \frac{\partial \rho}{\partial x} = \rho \lambda h_o \Phi \quad (3)$$

Generically, (2) describes the flow depth profile and (3) describes the change in density that accompanies the loss of volatiles during the emplacement of the flow. These equations must be supplemented with appropriate boundary conditions at the vent and solved simultaneously.

To obtain explicit mathematical solutions of (2) and (3), we must consider specific forms for the volume flow rate, q . Many theoretical lava flow modeling studies have assumed a Newtonian rheology for simplicity. The Newtonian flow rate per unit width is

$$q = \frac{g \sin \theta(x) h(x, t)^3}{3 \nu(x)} \quad (4)$$

where $\nu(x)$, the kinematic viscosity, is taken as an arbitrary function of distance from the source.

The validity of the Newtonian flow rate for modeling actual lava flows has never been firmly established. Other theoretically derived forms, e.g., the flow rate for a Bingham rheology (Skelland, 1967), and empirical forms for the volume flow rate (e.g., Baloga et al., 1995; Bruno et al., 1996; Glaze and Baloga, 1998) are admissible candidates. In order to bound the thickness and density profiles resulting from other choices of flow rate, we also consider a linear flow rate per unit width:

$$q = \frac{g \sin \theta(x) h(x,t)}{\alpha(x)} \quad (5)$$

We will refer to this flow rate as the “Basal Glide” model. This flow rate simply increases directly as more non-deforming lava is added on top of a thin fluid basal layer. Readers may recognize this flow rate as a proportionality to the basal shear stress of the flow, divided by a function, $\alpha(x)$, that characterizes the resistance to flow as a function of distance and has dimensions of time⁻¹.

When either (4) or (5), (or any other flow rate) are substituted into (2) and (3), explicit solutions for the thickness and density profiles can be obtained once the volatile loss function is specified. In what follows, we will show only the derivations for the Newtonian case and discuss selected examples for the Basal Glide model.

General Steady State Solutions

We now consider the steady state where the flow thickness, h , is a function only of distance and there are no time-dependent conditions at the vent itself. We will assume the slope is constant, although all results are readily extended for a variable slope. Integration of the volume conservation (2) using (4) leads to the general solution for the thickness profile

$$h(x) = h_o \left(\frac{v(x)}{v_o} \right)^{1/3} \left(1 - \frac{1}{L_\rho} \int_o^x \Phi dx \right)^{1/3} \quad (6)$$

where L_ρ is the length scale for the density change and is defined as

$$L_\rho = \frac{g \sin \theta h_o^2}{3 \lambda v_o} \quad (7)$$

See Table 2 for the definition of the length scale corresponding to the Basal Glide model. We can find the general steady state solution for the density profile *for any flow rate* by integrating (3) with the result

$$\rho(x) = \rho_o e^{\lambda h_o \int_0^x q(x)^{-1} \Phi(h,x) dx} \quad (8)$$

Further progress in evaluating the density is obtained by noting that (6) and (7) allow us to rewrite the Newtonian flow rate in (4) as

$$q(x) = L_\rho \lambda \frac{h(x)^3}{h_o^2} \frac{v_o}{v(x)} \quad (9)$$

Now, if we use the solution for $h(x)$ in (6) and substitute it into (9), we find that the term under the integral in (8) can be rewritten as

$$\lambda h_o \frac{\Phi(h,x)}{q(x)} = \frac{1}{L_{\rho}} \frac{\Phi(h,x)}{1 - \frac{1}{L_{\rho}} \int_0^x \Phi(h,x) dx} \quad (10)$$

Substituting (10) into (8) and integrating,

$$\rho(x) = \rho_o e^{-\ln \left(1 - \frac{1}{L_{\rho}} \int_0^x \Phi(h,x) dx \right)} \quad (11)$$

Simplifying (11), the general solution for the density becomes

$$\rho(x) = \frac{\rho_o}{1 - \frac{1}{L_{\rho}} \int_0^x \Phi(h,x) dx} \quad (12)$$

This interesting result indicates we can always find the steady state density profile once we know the rate of degassing as a function of flow thickness and distance. Conversely, this suggests that the cumulative rate of degassing can be inferred from systematic field measurements of density while the flow is active.

In Table 2, we show the corresponding results for the Basal Glide model. The reader can verify that the density profile obtained by the method above is identical to (12). From the form of the solution in (12), we can see that as long as the degassing is a function only of distance, i.e., $\Phi = \Phi(x)$, the change in density along the flow path is independent of the functional form of the viscosity, or resistance to flow. In contrast, if the degassing is a function of flow depth as well as distance (i.e., $\Phi = \Phi(h,x)$), the rheologic dependences in either (4) or (5) will influence the character

of the density change along the flow path.

3. PRACTICAL CONSTRAINTS FROM MAUNA LOA

The documentation of the 1984 eruption of Mauna Loa provides the most comprehensive data set for estimating the needed parameters for the model or prescribing reasonable choices. The main flow of the 1984 Mauna Loa eruption emplaced a 25 km long, well-defined solitary lobe (the “1 Flow”) in 4 days. An additional advance of 2 km occurred over the next day, concurrent with a major upstream breakout.

Over the life of the eruption lava density near the vent ranged from 510 to 1830 kg m⁻³ with spatter values as low as 330 kg m⁻³ [Lipman and Banks, 1987]. In general, the density near the vent decreased with time. Significant changes in density were also measured at different stations along the path of the flow, ranging from 530 to 2600 kg m⁻³ [Moore, 1987]. The 1A flow broke out toward the end of the emplacement of the 1 flow. The breakout of the 1A was attributed to an upstream blockage of the 1 Flow, while lava discharge from the vent continued at a fairly constant rate. The 1A flow was emplaced in just over 7 days and is approximately 13 km long with its terminus near that of the 1 flow. It appears that lava supplying the 1A flow was mostly degassed prior to reaching the breakout location approximately a 12 km from the vents [Lipman and Banks, 1987].

In this work, we will focus on the density difference between the vent and the front of an isolated flow lobe. As a reference, we will consider a hypothetical 25 km flow that has a thickness

of 4 m at the vent and is emplaced on a 4 degree slope in 5 days. We will nominally use 15 - 20 m as the thickness of the emplaced flow at the front. This thickness range is comparable to that observed at the front of the 1A flow.

Based on information in Lipman and Banks [1987] and Moore [1987] for the 1 and 1A flows, we consider a final density of 2600 kg m^{-3} as a reasonable choice for the density at the front of the flow. We will use this value as the final density and consider 3 choices for initial densities: 2000 kg m^{-3} , 1500 kg m^{-3} , and 600 kg m^{-3} . The first choice shows what happens to the density and thickness profiles if there is very modest degassing, such as might have occurred for the 1A flow. Our extreme case of 600 kg m^{-3} is in the low range of vent samples from the 1984 Mauna Loa eruption [Lipman and Banks, 1987]. Such initial densities could result from highly gas-charged lava as fountaining subsides. Our extreme value of 600 kg m^{-3} is also consistent with Moore [1987]. In that work, Moore inferred that the initial density must have been quite low to account for the apparent decrease in volumetric flow rate as a function of distance from the vent. We also consider the intermediate case of 1500 kg m^{-3} and compare all results to the case of no degassing during emplacement.

We will use two forms of models to describe how the viscosity changes with distance from the vent, a linear viscosity increase

$$v(x) = v_o \left(1 + x/L_v\right) \quad (13)$$

and an exponential viscosity increase

$$\nu(x) = \nu_o e^{x/L_v} \quad (14)$$

where L_v is the viscosity length scale. Note that the viscosity function will vary over the flow path according to a separate length scale that characterizes the rheologic change. This length scale, which we will call L_v , depends on different processes such as cooling or crystallization. Thus it must be specified or determined independent of the degassing scale by separate theoretical or empirical analyses.

There is abundant field, theoretical, and experimental literature suggestive of such increases in viscosity during flow emplacement (e.g., Einarsson, 1949; Minikami, 1951; Shaw, 1968; Danes, 1972; Harrison and Rooth, 1976; Pinkerton and Sparks, 1978; Baloga and Pieri, 1986; Fink and Zimbelman, 1986; Crisp and Baloga, 1990, 1994; Crisp et al., 1994; Glaze and Baloga, 1998; Cashman et al., 1999; Peitersen, 1999). Moore [1987] estimated apparent viscosity increases in excess of two orders of magnitude along the 1A flow, based on flow dimensions and theoretical calculations. This possibility is supported by crystallization measurements (Crisp et al., 1994). Studies of flows at Kilauea (Fink and Zimbelman, 1986, 1990) suggest comparable viscosity increases. Other recent studies of Puu Oo flows suggest the possibility of up to approximately a 3-orders of magnitude increase during the emplacement of Episode 2 (Baloga et al., 1998; Glaze and Baloga, 1998). The detailed nature of the viscosity increases during the emplacement of actual flows is difficult to assess. However, we consider the models shown in (13) and (14) to be representative of the literature cited above.

4. EXAMPLES

Because the rate of degassing from active flows is presently unknown, we will investigate two plausible models for the degassing function appearing in (2). One case assumes a constant rate of volatile loss. The other assumes the rate is proportional to the local volume of lava. We now consider some illustrative examples for each of these cases using the reference flow parameters discussed in the previous section.

Constant Degassing: $\Phi = 1$

In the simplest case, the rate of degassing along the flow path is constant, regardless of the flow thickness:

$$\Phi = 1 \tag{15}$$

In this case, we can easily evaluate the integral in (6) and see that the thickness profile is given by

$$h(x) = h_o \left(\frac{v(x)}{v_o} \right)^{1/3} \left(1 - x/L_p \right)^{1/3} \tag{16}$$

The functional form of (16) reflects the competition between an increasing flow resistance and an increasing density. In general, an increasing viscosity will try to thicken the flow, whereas the degassing term will try to thin the flow as it advances.

The density solution is easily determined from (12) to be:

$$\rho(x) = \frac{\rho_o}{1 - x/L_p} \quad (17)$$

It is interesting to note that the Basal Glide solution for $\rho(x)$ in Table 2 is identical in form to (17). The solutions differ only by the definitions of L_p . This implies that, for a constant rate of degassing, the density change along the profile is independent of the flowrate dependence on h . Specifically, the Newtonian, the Basal Glide, and any other flow rate models that are functions of flow depth, give the same result.

We do not know the bulk degassing rate constant λ for any actual lava flows at the present time. This prevents us from determining L_p for either of the flow rates under consideration. However, we can obtain an estimate of the density length scale by solving (17) for L_p at the cessation of flow advance

$$L_p = \frac{x_f}{1 - \rho_o/\rho_f} \quad (18)$$

where x_f is the final length of the flow.

Tables 3 and 4 contain formulas for estimating the length scales for density changes for the

two flow rates considered here, and different degassing and viscosity models. Using our reference values for vent and final densities, flow length, and initial and final flow thickness, we can now compute the density and thickness profiles.

Figure 1 shows the density changes for constant degassing with the 3 different boundary conditions for initial density at the vent. Note that these curves are independent of both the form of the flow rate and the character of the rheologic change along the flow path. Except for the extreme case of 600 kg m^{-3} , the density increase is approximately linear from the vent to the flow front. It is interesting, however, that in the extreme case, the rate of density change increases rapidly toward the front.

Figure 2 shows the flow thickness profiles for constant degassing, Newtonian flow rate, a linear increase in the viscosity along the flow path, and the three plausible reference values for the lava density at the vent. The profile for no degassing is also shown for comparison. The profiles were computed using the formulas in Table 3. We have selected the viscosity length scale such that there is a two order of magnitude increase in viscosity over the nominal 25 km length of the flow. This viscosity length scale results in a flow that thickens to approximately 18 m at the front in the case of no degassing. The figure shows that modest degassing results in about a 4 m change in flow depth toward the front compared to the case of no degassing. In the extreme case, there is actually a rollover in the profile and an 8 m difference in flow front thickness compared to the constant density case.

Figure 3 shows the flow thickness profiles for constant degassing, the Basal Glide model, a linear increase in the rheology along the flow path, and the three boundary conditions for density at the vent. The profile for no degassing is also shown. The profiles were computed using the formulas in Table 3. For comparison with the Newtonian case shown in Figure 2, we have selected the rheology length scale so that the flow thickens to approximately 18 m at the front in the case of no degassing. The choice of initial density has a more dramatic influence on the shape of the flow profile. Even the intermediate degassing case of $\rho_o = 1500 \text{ kg m}^{-3}$ decreases the thickness at the flow front by a factor of two. For a constant rate of degassing, the flow thickness profile is very sensitive to the choice of flow rate and the initial density.

Depth-Dependent Degassing: $\Phi = h/h_o$

We now consider a degassing function that is dependent on the volume of lava at any position along the flow. Thus, for a flow with constant width and a control volume with length dx , we take the degassing function as

$$\Phi(h,x) = \frac{h(x)}{h_o} \quad (19)$$

To find the steady state solution for the flow profile, we can use integral methods of solution for (6) or simply re-write (2) with (19) as

$$\frac{d}{dx} \left(\frac{g \sin \theta h^3}{3 \nu} \right) = -\lambda h \quad (20)$$

To do the integration, we make the following transformations for h and v :

$$\xi = \frac{h}{v^{1/3}}; \quad y(x) = \int_0^x v^{1/3} dx \quad (21)$$

so that (20) becomes

$$\xi \frac{d\xi}{dy} = \frac{-h_o^2}{3 v_o L_\rho} \quad (22)$$

Elementary integration of (22) and transformation back to the original variables results in the expression for the thickness profile

$$h(x) = h_o \left(\frac{v(x)}{v_o} \right)^{1/3} \left(1 - \frac{2}{3 L_\rho} \int_0^x \left(\frac{v(x)}{v_o} \right)^{1/3} dx \right)^{1/2} \quad (23)$$

With (23), the density can be found directly from the general solution in (8)

$$\rho(x) = \rho_o e^{\frac{h_o^2}{v_o L_\rho} \int_0^x \frac{v}{h^2} dx} \quad (24)$$

The nonlinear dependence of the Newtonian flow rate on h results in a density change that now depends on the changes in the viscosity and flow depth. With (23), the integral in (24) can be done explicitly for an arbitrary viscosity change

$$\rho(x) = \rho_o \left(1 - \frac{2}{3L_{\rho_o}} \int_0^x \left(\frac{v(x)}{v_o} \right)^{1/3} dx \right)^{-3/2} \quad (25)$$

where the density again clearly depends on the form and length scale for the viscosity change. We are fortunate that the integrals leading to (25) can be done in the general case. This important result means we can compute the density profile directly from knowledge of the viscosity change.

We can estimate the length scale of the degassing by solving (25) for L_{ρ} , and evaluating the result at the flow terminus:

$$L_{\rho} = \frac{\frac{2}{3} \int_0^{x_f} \left(\frac{v(x)}{v_o} \right)^{1/3} dx}{1 - \left(\frac{\rho_o}{\rho_f} \right)^{2/3}} \quad (26)$$

For linearly increasing viscosity of the form given in (13), we can estimate the degassing length scale from field data by

$$L_{\rho} = \frac{L_v \left[(1 + x_f/L_v)^{4/3} - 1 \right]}{2 \left[1 - (\rho_o/\rho_f)^{2/3} \right]} \quad (27)$$

We can now solve (25) for the density change,

$$\rho(x) = \frac{\rho_o}{\left[1 - \frac{L_v}{2L_\rho} \left((1+x/L_v)^{4/3} - 1\right)\right]^{3/2}} \quad (28)$$

as well as (23) for the thickness profile

$$h(x) = h_o (1+x/L_v)^{1/3} \left[1 - \frac{L_v}{2L_\rho} \left((1+x/L_v)^{4/3} - 1\right)\right]^{1/2} \quad (29)$$

A variety of other estimates of the density length scale, as well as solutions for density and flow thickness, for other rheologies and the Basal Glide model appear in Table 4.

Figure 4 shows the density change for a Newtonian flow rate with a viscosity that increases by 2 orders of magnitude and a depth-dependent rate of degassing. We have selected the viscosity length scale to produce the same flow front thickness as in Figure 2 when there is no degassing. There are differences from the constant degassing case, but they appear to be small compared to the constant degassing case. This is to be anticipated because we have fixed the densities at the vent, the final density, and chosen the viscosity length scale so that the constant density case attains a fixed value. Other options for fixing the parameters and presenting the model results appear in the Discussion.

Figure 5 shows the thickness profiles corresponding to the curves in Figure 4. Quantitatively, we see the same influence of depth-dependent degassing as before. For extreme values of volatile loss and density change, the depth at the front can differ from the constant density case by as much

as 8 m and the profile again features gentle rollover in the thickness.

Fig 6 shows the thickness profiles for the Basal Glide model with depth-dependent degassing and the same parametric constraints as before. Because the initial and final densities and thicknesses have been fixed, there are only minor differences between these profiles and those obtained from the constant degassing case (See Fig. 3).

Figure 7 shows two thickness profiles for the Newtonian flowrate with a depth-dependent rate of degassing and the exponential viscosity model in (14). L_v has been chosen as 5.4 km to make the final flow thickness 19 m when there is no degassing. This is equivalent to a two-order increase in magnitude over 25 km. The profile with no degassing shows the anticipated exponential increase in thickness. The lower profile results from the initial lava density of 600 kg m^{-3} . It differs significantly from the constant density profile and features a modest distal rollover.

5. DISCUSSION

When degassing causes a significant difference in the flow thickness, compared to the case of a constant density, there can be a corresponding difference in emplacement times. As an example, we will take a flow that travels the nominal 25 km in 5 days on a slope of 4 degrees when there is no degassing. We have computed the flow advance rates for the two cases shown in Figure 7. The local flow velocity is obtained from the definition, $q = h(x)u(x)$.

The results are shown in Figure 8. The lower curve is the advance rate for no degassing and

the upper curve results from the extreme density change. The loss of volatiles during emplacement produces a dramatic change on the emplacement time. This example requires 8 days, significantly longer than the constant density case, to traverse the 25 km. This difference is due to the accumulated differences in flow thickness. The exponential increase in viscosity results in an almost linear advance rate. However, the extreme degassing case has an exponential character.

The sensitivity of flow emplacement to degassing is clearly evident in Figure 8. The relatively rapid change in viscosity magnifies the influence of degassing in thinning the flow. Because the Newtonian flow rate has such a strong effect on flow velocity (i.e., an h^2 dependence), it magnifies the combined influences of viscosity and density changes.

The examples in Section 4 were all constructed to meet highly restrictive endpoint constraints. Specifically, the parameters were selected so that the flow thickens from 4 m to 18 or 19 m for a constant density. Regardless of the density at the vent, the final density was required to be 2600 kg m^{-3} . Imposing such restrictions on the parameters minimizes the differences in the appearance of the thickness profiles in Section 4.

It is intuitively obvious that degassing must, in some sense, mask the thickening of a flow due to a viscosity increase. This is difficult to unravel based on the presentation of the previous examples. Consequently, we now pose the problem from a different perspective than that of Section 4. Suppose we select the final flow thickness to be 19 m *when the maximum density change occurs*. Then, how would the thickness profiles differ for the same viscosity change and lesser

density changes at the vent?

To answer this question, we will use the Newtonian flow rate, a depth-dependent rate of degassing, and an exponential increase in viscosity. For our reference flow, we must now select the length scale for the viscosity increase to be 4.1 km so that the flow thickens to 19 m when the density starts at 600 kg m^{-3} . The resulting thickness profiles are shown in Figure 9. Now the thickness profile for a constant density increases to 31 m at the front. Even the case of a 1500 kg m^{-3} initial density exceeds 25 m at the flow front.

This change in perspective highlights the importance of degassing during emplacement. We also note here that the use of a 4.1 km length scale for the viscosity change causes the relative viscosity to increase by a factor of 445 along the path of the flow, whereas the curves shown in Figure 7 have only two orders of magnitude. Thus, if we only know the initial and final flow thickness without the total density change, we cannot accurately assess the rheologic change.

Finally, we remark that our method for estimating the density length scale also provides an estimate for the elusive rate constant λ . Such estimates are obtained by equating the definition of the density length scale to the formula for its estimation. For example, for a constant rate of degassing and a Newtonian flow rate, one can use (7) and (18) to obtain different estimates of λ for each set of density values. For the example shown in Figures 1 and 2, we obtain λ^{-1} values of 2.7, 5.0, and 9.1 days for the initial densities of 600, 1500, and 2000 kg m^{-3} , respectively. As expected, these values are comparable to the nominal emplacement duration of 5 days with the magnitude of

the effect on the thickness profiles being proportional to λ .

Some improvement in our understanding of the degassing process might be obtained by formulating an independent governing equation that would predict the form of Φ in eq 2. Such a formulation might be based on bubble nucleation, coalescence, and migration, circulation and mixing within the flow, and similar factors, which would change along the length of a flow. Because these processes would still require empirical parameters, it is not clear whether such an approach would be worthwhile.

6. CONCLUSIONS

We have presented a model of a lava flow to examine the combined influence of density and viscosity changes during emplacement on the longitudinal thickness and density profiles. Our formulation can accommodate different types of flow rates and models of volatile loss during emplacement. We have considered two endmember flow rates, Newtonian and Basal Glide, with cubic and linear dependences on flow thickness, respectively. We have considered two types of volatile loss rates, one that is constant and another that depends on the thickness of the flow. Linear and exponential models for the change in rheology with distance have been investigated.

In the steady state, general solutions for the thickness and density profiles can be readily obtained. These solutions show that, for a constant or spatially dependent rate of volatile loss, the density profile is independent of the form of the flowrate dependence on h and the nature of the

rheologic change with distance. Specifically, the Newtonian and Basal Glide models produce the same density profile.

Flow thickness profiles are sensitive to the choice of flow rate and the initial density, regardless of the form of the degassing function. For identical boundary conditions, the nature of the flow rate can significantly affect the shape of the profile as well as the flow front thickness. Both the Newtonian and Basal Glide models produce plausible thickness profiles resembling those observed in the field. We expect that other reasonable choices for flow rate would produce similar results.

When the rate of volatile loss depends on the flow thickness, the density profile depends explicitly on the way the rheology changes along the flow path, even for a flow rate that depends linearly on the flow thickness. This contrasts with the case when the degassing is constant or has only a spatial dependence. Time-dependent solutions can also be readily obtained from our governing equations and results will be reported elsewhere.

In all cases, density increases during emplacement counter the tendency of a flow to thicken due to increases in viscosity or resistance to flow with distance. The steady state density profiles are relatively insensitive to the form of the flow rate and, even in the case of a depth-dependent degassing rate, the nature of the rheologic change. Degassing effects on the thickness of a lava flow can be significant when there is a large difference between the density at the vent and the flow front. With extreme density differences, the loss of volatiles can cause a rollover in the thickness profile

as the degassing term overpowers the viscosity term. Rollover occurs closer to the vent for higher rates of degassing and also for higher rates of viscosity increase along the path of the flow. For depth-dependent degassing, an increase in viscosity acts to thicken the flow, which increases the rate of degassing. This mitigates the thickening influence of an increasing viscosity. For parameters comparable to those of the large 1984 Mauna Loa flows, the thickness of the flow front can be influenced by as much as 60% by volatile losses during emplacement.

Degassing during emplacement can also have an effect on flow velocity and hence transit times. For a Newtonian flow rate the local flow velocity depends on the squared thickness of the flow. Consequently, decreases in thickness due to degassing can affect the advance rate significantly. This effect is most pronounced when the degassing is rapid enough to produce a rollover in the longitudinal profile. For large basaltic flows with parameters comparable to those from the 1984 Mauna Loa eruption, the difference in emplacement times between extreme and negligible degassing can be as much as a factor of 60%.

If we do not account for density changes, viscosity increases computed from thickness changes can be in error by an order of magnitude or more. This implies the need for systematic in-situ measurements of lava density from quenched field samples. Such measurements can then be used to determine the form of the volatile loss function and the appropriate rate constants. While systematic measurements of lava density as functions of time and distance are preferred, even relatively crude estimates of effused and emplaced lava densities are of use in estimating the amount of degassing.

As both field studies and our steady state results suggest, understanding time-dependent effects is essential for a more complete description of the emplacement of such flows. Variations in the underlying topography and flow width and interactions between volatile losses and rheologic changes are also important factors. Nevertheless, our results highlight the fruitfulness of understanding the role of degassing and density changes on the emplacement of lava flows in terrestrial and planetary settings.

ACKNOWLEDGMENTS

The authors would like to respectfully acknowledge the late Henry Moore for pointing out the problem of degassing and density changes during emplacement well over a decade ago. The work by S. Baloga, L. Glaze, and M. Peitersen was supported by the NASA Planetary Geology and Geophysics Program, grant NAG5-7251. The work by J. Crisp was carried out at the Jet Propulsion Laboratory, California Institute of Technology, under a contract to the National Aeronautics and Space Administration.

REFERENCES

- Baloga, S.M and D.C. Pieri, Time-dependent profiles of lava flows, *J. Geophys. Res.*, *91*, 9543- 9552, 1986.
- Baloga, SM., P D Spudis, and J. E. Guest, The dynamics of rapidly emplaced terrestrial lava flows and implications for planetary lava flows, *J. Geophys. Res., Solid Earth*, *100*: No. B12,24,509-24,519, 1995.
- Baloga, S.M., L.S. Glaze, J.A. Crisp, and S.A. Stockman, New statistics for estimating the bulk rheology of active lava flows: Puu Oo examples, *J. Geophys. Res.*, *103*, 5133-5142, 1998.
- Bottinga, Y., D. Weill, and P. Richet, Density calculations for silicate liquids. 1. Revised method for aluminosilicate compositions, *Geochim. Cosmochim. Acta*, *46*: 909-919, 1982.
- Bruno, BC, S M. Baloga and GJ Taylor, Modeling gravity-driven flows on an inclined plane, *J. Geophys. Res.*, *101*, 11,565-11577, 1996.
- Cashman, K.V., M.T. Mangan, and S. Newman, Surface degassing and modifications to vesicle size distributions in active basalt flows, *J. Volcanol. Geotherm. Res.*, *61*, 45-68, 1994.
- Cashman, K.V., C. Thornber, and J.P. Kauahikaua, Cooling and crystallization of lava in open channels, and the transition of Pahoehoe Lava to A'a, *Bull. Volcanol.*, *661*, 306-323, 1999.
- Crisp, J. and S. Baloga, A model for lava flows with two thermal components, *J. Geophys. Res.*, *95*, 1255-1270, 1990.
- Crisp, J. and S. Baloga, Influence of crystallization and entrainment of cooler material on the emplacement of basaltic aa lava flows, *J. Geophys. Res.*, *99*, B6, 11,819-11,831, 1994.
- Crisp, J., K.V. Cashman, J.A. Bonini, S.B. Hougén, and D.C. Pieri, Crystallization history of the 1984 Mauna Loa lava flow, *J. Geophys. Res.*, *99*, 7177-7198, 1994.

- Danes, Z.F., Dynamics of lava flows, *J. Geophys. Res.*, 77, 1430-1432, 1972.
- Einarsson, T., G. Kjartansson, and S. Thorarinsson (Eds.), *The eruption of Hekla 1947-1948*, Visindafelg Islendinga, Reykjavik, 1949.
- Fink, J.H. and J.R. Zimbelman, Rheology of the 1983 Royal Gardens basalt flows, Kilauea Volcano, Hawaii, *Bull. Volcanol.*, 48, 87-96, 1986.
- Fink, J.H. and J.R. Zimbelman, Longitudinal variations in rheological properties of lavas: Puu Oo basalt flows, Kilauea volcano, Hawaii, in Fink, J.H. (Ed.), *Lava Flows and Domes: Emplacement Mechanism and Hazard Implications*, Springer-Verlag, Berlin, New York, 157-173, 1990.
- Glaze, LS and SM Baloga, Dimensions of Puu Oo lava flows on Mars, *J. Geophys. Res.*, 103, 13,659-13,666, 1998.
- Harrison, C.G.A., and C. Rooth, The dynamics of flowing lavas, in *Volcanoes and the Tectonosphere*, pp. 103-113, University of Tokyo, Tokyo, 1976.
- Hon, K., J. Kauahikaua, R. Denlinger, and K. Mackay, Emplacement and inflation of pahoehoe sheet flows: Observations and measurements of active lava flows on Kilauea Volcano, Hawaii, *Geol. Soc. Bull.*, 106, 351-370, 1994.
- Lipman, P.W. and N.G. Banks, Aa flow dynamics, Mauna Loa 1984, in Decker, R.W., T.L. Wright, and P.H. Stauffer, *Volcanism in Hawaii*, U. S. Geol. Surv. Prof. Pap., 1350, 1527-1567, 1987.
- Malin, M.C., Lengths of Hawaiian lava flows, *Geology*, 8, 306-308, 1980.
- Minikami, T., On the temperature and viscosity of the fresh lava extruded in the 1951 Oosima eruption, *Bull. Earthquake Res. Inst. Univ. Tokyo*, 29, 487-498, 1951.

- Moore, H. J., A geological evaluation of proposed lava diversion barriers for the NOAA Mauna Loa Observatory, Mauna Loa Volcano, Hawaii, and some recommendations: *U. S. Geol. Surv. Open-File Report 82-314*, 17 pp, 1982.
- Moore, H.J., Preliminary estimates of the rheological properties of 1984 Mauna Loa lava, in Decker, R.W., T.L. Wright, and P.H. Stauffer, *Volcanism in Hawaii, U. S. Geol. Surv. Prof. Pap., 1350*, 1569-1588, 1987.
- Peitersen, M.N., Downflow width behavior of Martian and terrestrial lava flows, *J. Geophys. Res., 104*, 8473-8488, 1999.
- Pinkerton, H., and R.S.J. Sparks, Field measurements of the rheology of lava, *Nature*, 276, 383-385, 1978.
- Prousevitch, A.A., D.L. Sahagian, and A.T. Anderson, Dynamics of diffusive bubble growth in magmas: Isothermal case, *J. Geophys. Res., 98*, 22,283-22,307, 1993.
- Rhodes, J.M., Geochemistry of the 1984 Mauna Loa Eruption: Implications for magma storage and supply, *Jour. Geophys. Res., 93*: 4453-4466, 1988.
- Shaw, H.R., T.L. Wright, D.L. Peck, R. Okamura, The viscosity of basaltic magma: An analysis of field measurements in Makaopuhi lava lake, *Hawaii, Am. Jour. Sci., 266*, 225-263, 1968.
- Skelland, A.H.P., *Non-Newtonian Flow and Heat Transfer*, 469pp., John Wiley, New York, 1967.
- Sparks, R.S.J. and H. Pinkerton, Effect of degassing on rheology of basaltic lava, *Nature*, 276, 385-386, 1978.
- Sparks, R.S.J., The dynamics of bubble formation and growth in magmas: a review and analysis, *J. Volcanol. Geotherm. Res., 3*, 1-37, 1978.
- Taylor, B.E., J.C. Eichelberger, and H.R. Westrich, Hydrogen isotopic evidence of rhyolitic magma

Table 1. Definition of Symbols

Symbol	Definition
g	gravitational field strength ($= 9.8 \text{ m s}^{-2}$)
h	variable flow depth (m)
h_0	initial flow depth ($x = 0, t = 0$)
L_α	BGM rheology length scale (m)
L_v	Newtonian viscosity length scale (m)
L_ρ	density length scale (m)
q	volumetric flow rate per unit width ($\text{m}^2 \text{ s}^{-1}$)
t	time (s)
$u(x)$	flow velocity (m s^{-1})
x	distance (m)
x_f	final flow length (m)
$y(x)$	transformation variable
$\alpha(x)$	BGM rheology function (s^{-1})
θ	average slope (degrees)
λ	rate constant for volumetric loss (s^{-1})
$\nu(x)$	kinematic viscosity (m^2/s)
ν_0	initial kinematic viscosity, $\nu(x = 0)$
$\rho(x)$	density (kg m^{-3})
ρ_0	initial density, $\rho(x = 0)$
ρ_f	final density, $\rho(x = x_f)$
Φ	volatile loss function (dimensionless)
ξ	transformation variable

degassing during shallow intrusion and eruption, ?,1984.

Wadge, G., The variation of magma discharge during basaltic eruptions, *J. Volcanol. Geotherm. Res.*, 11, 139-168, 1981.

Wallace, P.J. and A.T. Anderson, Effects of eruption and lava drainback on the H₂O contents of basaltic magmas at Kilauea Volcano, *Bull. Volcanol.*, 59, 327-344, 1998.

Westrich, H.R., H.W. Stockman, and J.C. Eichelberger, Degassing of rhyolitic magma during ascent and emplacement, *J. Geophys. Res.*, 93, 6503-6511, 1988.

Wilson, L. and J. W. Head, Ascent and eruption of basaltic magma on the Earth and Moon, *J. Geophys. Res.*, 86, 2971-3001, 1981.

Table 3. Solutions for h , ρ , and L_p , for the constant degassing case, $\Phi = 1$, by rheology increase model and flow rate.

Rheo. Model/ Flow Rate	$h(x)$	$\rho(x)$	L_p (estimate)
Linear/Newt	$h(x) = h_o \left(1 + x/L_v\right)^{1/3} \left(1 - x/L_p\right)^{1/3}$	$\rho(x) = \frac{\rho_o}{1 - x/L_p}$	$L_p = \frac{x_f}{1 - \rho_o/\rho_f}$
Linear/BGM	$h(x) = h_o \left(1 + x/L_a\right) \left(1 - x/L_p\right)$	$\rho(x) = \frac{\rho_o}{1 - x/L_p}$	$L_p = \frac{x_f}{1 - \rho_o/\rho_f}$
Exp/Newt	$h(x) = h_o e^{x/3L_v} \left(1 - x/L_p\right)^{1/3}$	$\rho(x) = \frac{\rho_o}{1 - x/L_p}$	$L_p = \frac{x_f}{1 - \rho_o/\rho_f}$
Exp/BGM	$h(x) = h_o e^{x/L_a} \left(1 - x/L_p\right)$	$\rho(x) = \frac{\rho_o}{1 - x/L_p}$	$L_p = \frac{x_f}{1 - \rho_o/\rho_f}$

Table 2. General Solutions

	Newtonian	Basal Glide
Volume Flow Rate per Unit Width	$q = \frac{g \sin \theta h^3}{3 \nu}$	$q = \frac{g \sin \theta h}{\alpha}$
Density Length Scale	$L_\rho = \frac{g \sin \theta h_o^2}{3 \lambda \nu_o}$	$L_\rho = \frac{g \sin \theta}{\lambda \alpha_o}$
General Solution for $h(x)$	$h(x) = h_o \left(\frac{\nu(x)}{\nu_o} \right)^{1/3} \left(1 - \frac{1}{L_{\rho_o}} \int_0^x \Phi(h, x) dx \right)^{1/3}$	$h(x) = h_o \left(\frac{\alpha(x)}{\alpha_o} \right) \left(1 - \frac{1}{L_{\rho_o}} \int_0^x \Phi(h, x) dx \right)$
General Solution for $\rho(x)$	$\rho(x) = \frac{\rho_o}{1 - \frac{1}{L_{\rho_o}} \int_0^x \Phi(h, x) dx}$	$\rho(x) = \frac{\rho_o}{1 - \frac{1}{L_{\rho_o}} \int_0^x \Phi(h, x) dx}$

FIGURE CAPTIONS

- Figure 1. Density profiles for constant degassing ($\Phi = 1$) with $\rho_o = 2000, 1500$ and 600 kg m^{-3} . The density, ρ , and L_ρ were computed using the formulas in Table 3. These density profiles hold for any arbitrary volumetric flow rate. Except for the extreme case of 600 kg m^{-3} , the density increase is approximately linear from the vent to the flow front.
- Figure 2. Flow thickness profiles for constant degassing ($\Phi = 1$), Newtonian flow rate, a linear viscosity increase along the flow path, and $\rho_o = 2000, 1500$ and 600 kg m^{-3} . The profile for no degassing is also shown (uppermost curve). The profiles were computed using the Linear/Newt formula in Table 3.
- Figure 3. Flow thickness profiles for constant degassing ($\Phi = 1$), Basal Glide flow rate, a linear rheology increase along the flow path, and $\rho_o = 2000, 1500$ and 600 kg m^{-3} . The profile for no degassing is also shown (uppermost curve). The profiles were computed using the Linear/BGM formula in Table 3.
- Figure 4. Density profiles for depth-dependent degassing ($\Phi = h/h_o$), a Newtonian flow rate, a viscosity that increases linearly by 2 orders of magnitude, and $\rho_o = 2000, 1500$ and 600 kg m^{-3} . The density, ρ , and L_ρ were computed using the Linear/Newt formulas in Table 4. The viscosity length scale is selected to produce the same flow front thickness as in Figure 2 when there is no degassing.

Table 4. Solutions for h , ρ , and L_p , for the depth dependent degassing case, $\Phi = h/h_o$ by rheology increase model and flow rate.

Rheo Model/ Flow rate	$h(x)$	$\rho(x)$	L_p (estimate)
Linear/Newt	$h_o \left(1 + x/L_v\right)^{1/3} \left(1 - \frac{L_v}{2L_p} \left[\left(1 + x/L_v\right)^{4/3} - 1\right]\right)^{1/2}$	$\frac{\rho_o}{\left(1 - \frac{L_v}{2L_p} \left[\left(1 + x/L_v\right)^{4/3} - 1\right]\right)^{3/2}}$	$\frac{L_v \left[\left(1 + x_f/L_v\right)^{4/3} - 1\right]}{2 \left[1 - (\rho_o/\rho_f)^{2/3}\right]}$
Linear/BGM	$h_o \left(1 + x/L_\alpha\right) e^{-L_\alpha/2L_p \left[\left(1 + x/L_\alpha\right)^2 - 1\right]}$	$\rho_o e^{L_\alpha/2L_p \left[\left(1 + x/L_\alpha\right)^2 - 1\right]}$	$\frac{L_\alpha \left[\left(1 + x_f/L_\alpha\right)^2 - 1\right]}{2 \ln(\rho_f/\rho_o)}$
Exp/Newt	$h_o e^{x/3L_v} \left[1 - \frac{2L_v}{L_p} \left(e^{x/3L_v} - 1\right)\right]^{1/2}$	$\frac{\rho_o}{\left[1 - \frac{2L_v}{L_p} \left(e^{x/3L_v} - 1\right)\right]^{3/2}}$	$\frac{2L_v \left(e^{x_f/3L_v} - 1\right)}{1 - (\rho_o/\rho_f)^{2/3}}$
Exp/BGM	$h_o e^{x/L_\alpha - L_\alpha/L_p \left(e^{x/L_\alpha} - 1\right)}$	$\rho_o e^{L_\alpha/L_p \left(x/L_\alpha - 1\right)}$	$\frac{L_\alpha \left(e^{x_f/L_\alpha} - 1\right)}{\ln(\rho_f/\rho_o)}$

Figures 5. Thickness profiles for depth-dependent degassing ($\Phi = h/h_0$), a Newtonian flow rate, a viscosity that increases linearly by 2 orders of magnitude, and $\rho_0 = 2000, 1500$ and 600 kg m^{-3} . The profile for no degassing is also shown (uppermost curve). The profiles were computed using the Linear/Newt formula in Table 4. Quantitatively, there are only minor differences between these profiles and those obtained from the constant degassing case (Figure 2).

Figures 6. Thickness profiles for depth-dependent degassing ($\Phi = h/h_0$), the Basal Glide flow rate, a linearly increasing viscosity, and $\rho_0 = 2000, 1500$ and 600 kg m^{-3} . The profile for no degassing is also shown (uppermost curve). The profiles were computed using the Linear/BGM formula in Table 4. Quantitatively, there are only minor differences between these profiles and those obtained from the constant degassing case (Figure 3).

Figure 7. Thickness profiles for depth-dependent degassing ($\Phi = h/h_0$), a Newtonian flow rate, and an exponentially increasing viscosity. The upper and lower curves show constant density (no degassing) and $\rho_0 = 600 \text{ kg m}^{-3}$, respectively. The lower profile differs significantly from the constant density profile and features a modest distal rollover.

Figure 8. Advance rates for the two cases illustrated in Figure 7. The upper and lower curves correspond to the extreme density change and no degassing cases, respectively. The

loss of volatiles during emplacement produces a dramatic change in the emplacement time.

Figure 9. Thickness profiles for depth-dependent degassing ($\Phi = h/h_0$), a Newtonian flow rate, and an exponentially increasing viscosity. This figure differs from Figure 7 in that the length scale for the viscosity increase has now been selected such that the flow thickens to 19 m when $\rho_o = 600 \text{ kg m}^{-3}$. The profiles for no degassing (uppermost curve), and $\rho_o = 2000$ and 1500 kg m^{-3} are also shown.

FIGURE 1 Density: Constant Degassing

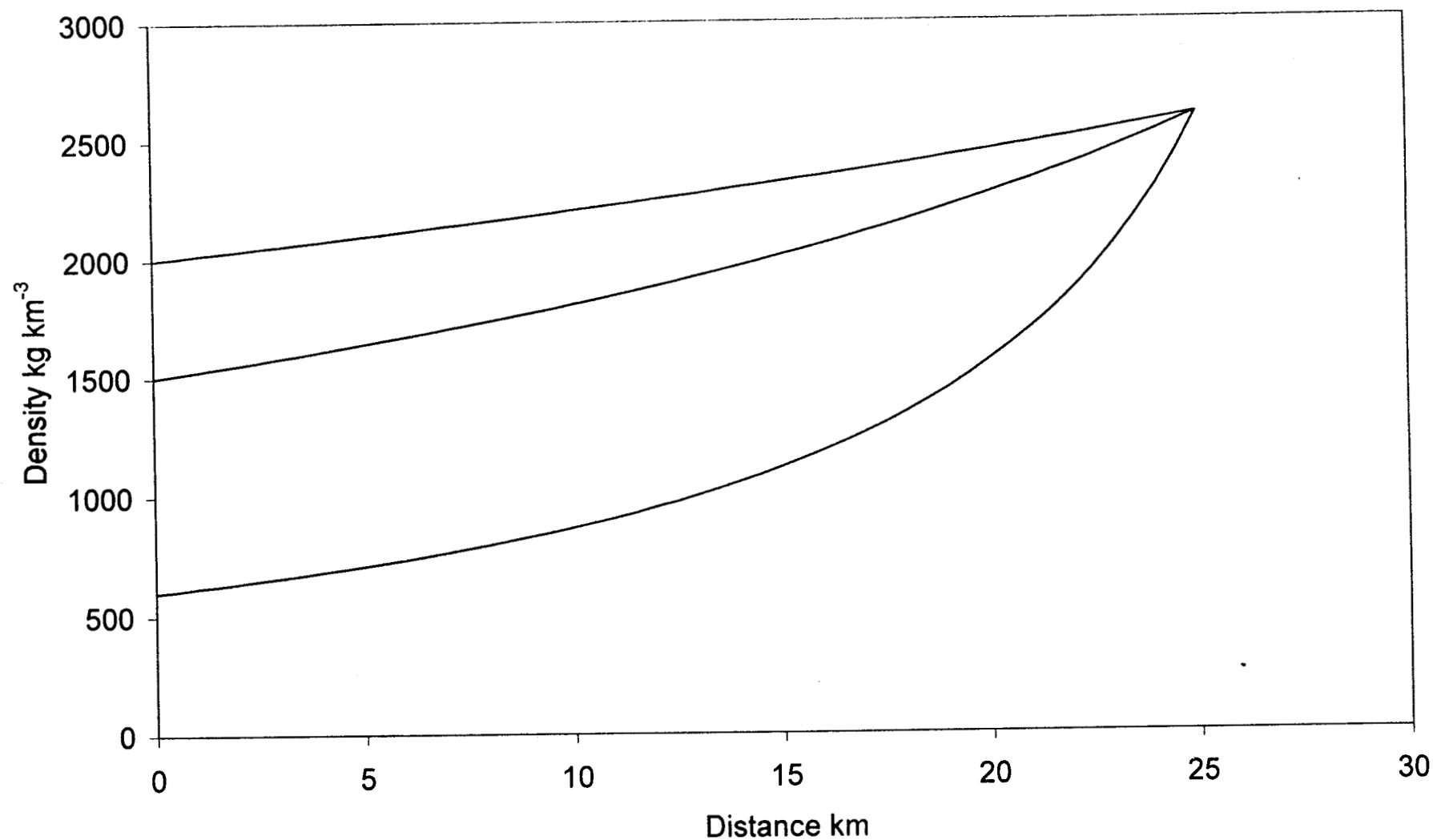


FIGURE 2 Thickness Profile: Constant Degassing Rates, Newtonian Flow Rate, Linear Viscosity

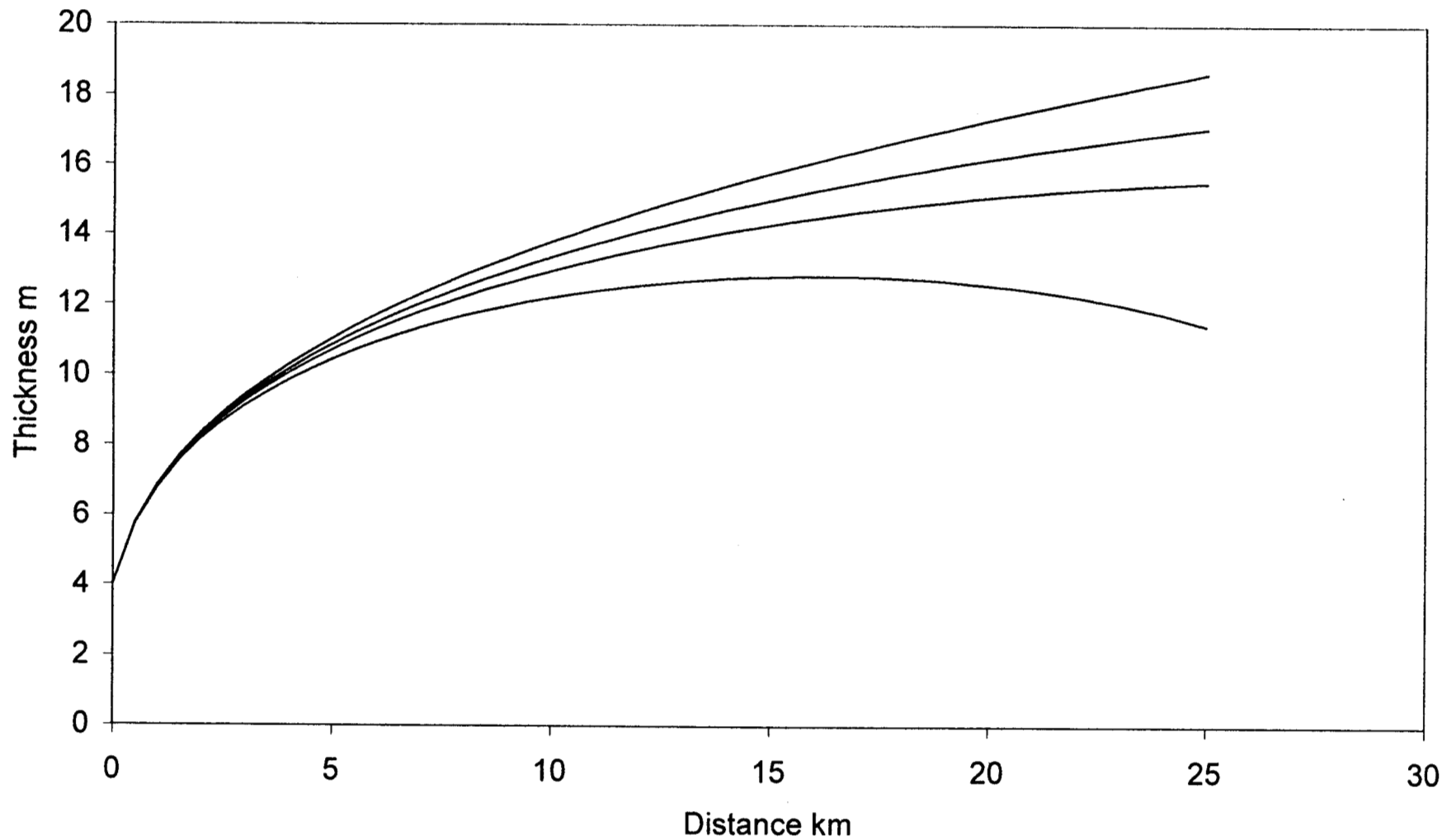


Figure 3 Thickness Profile: Constant Degassing Rates, Basal Glide Flow Rate, Linear Rheology

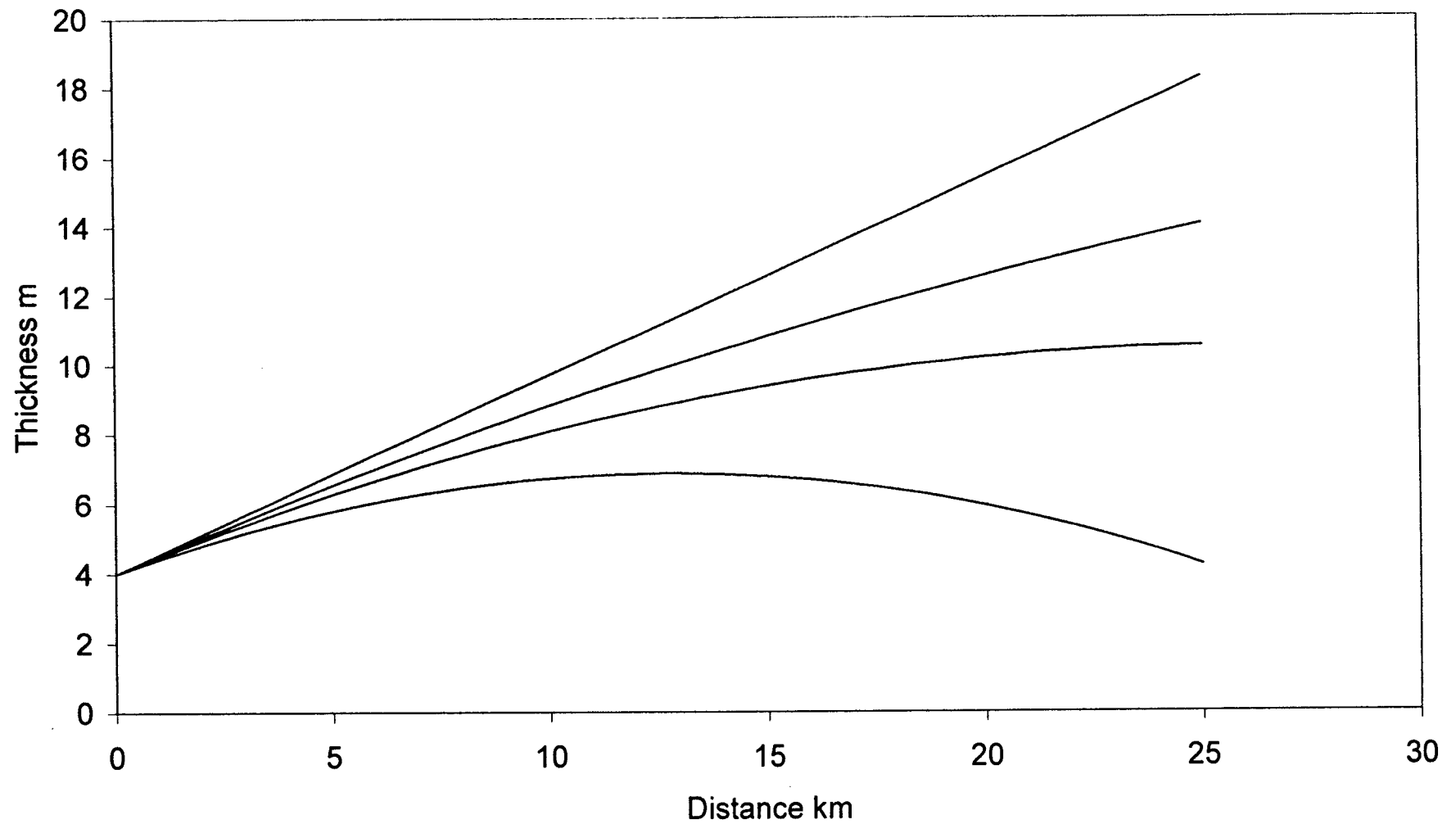


FIGURE 4 Density: Depth-dep degassing, Newtonian Flow Rate, Linear Visc

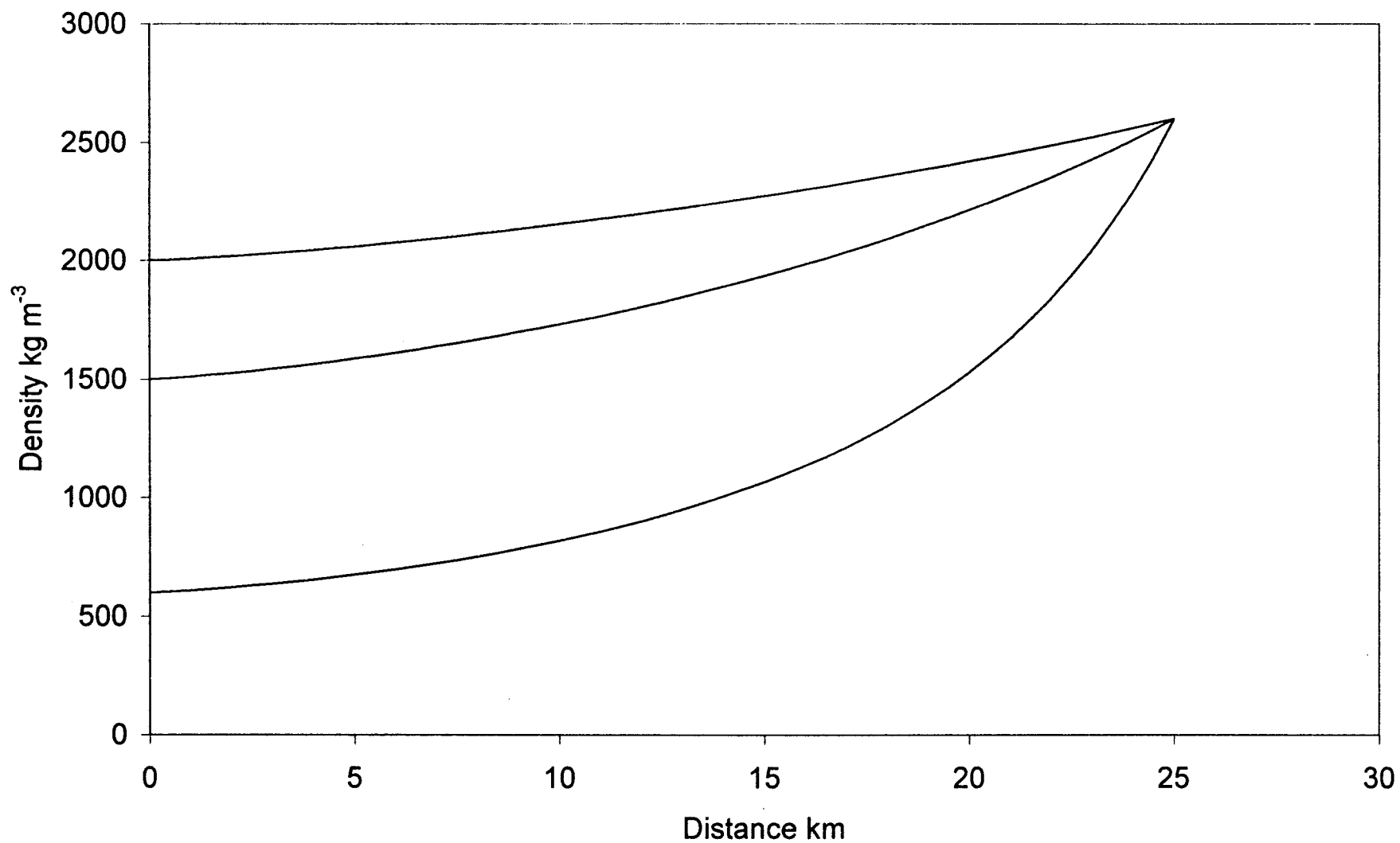


FIGURE 5 Thickness Profile: Depth-dep Degassing, Newtonian Flow Rate, Linear Viscosity

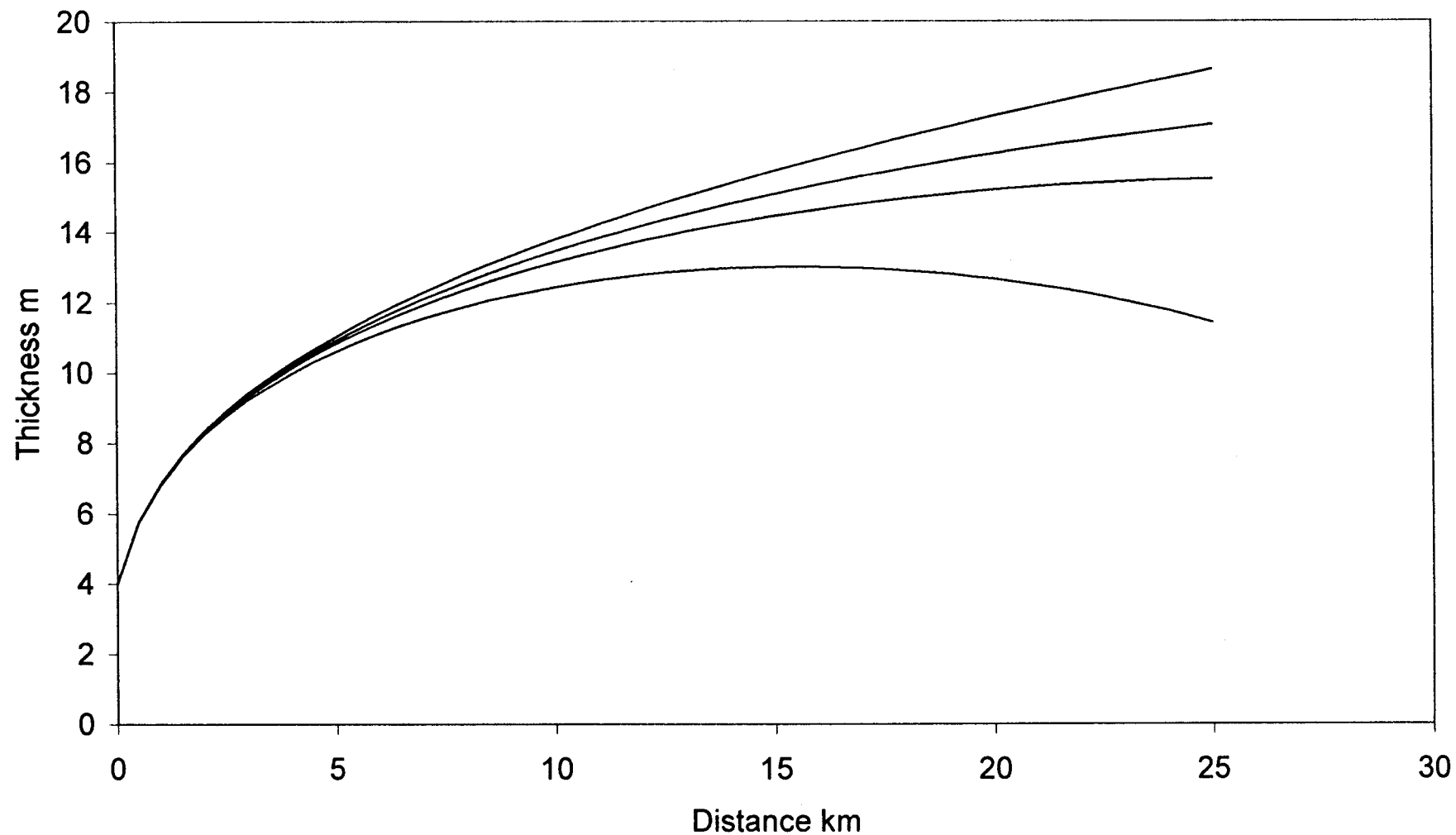


FIGURE 6 Thickness Profile: Depth-dependent Degassing, Basal Stress Model, Linear Rheology

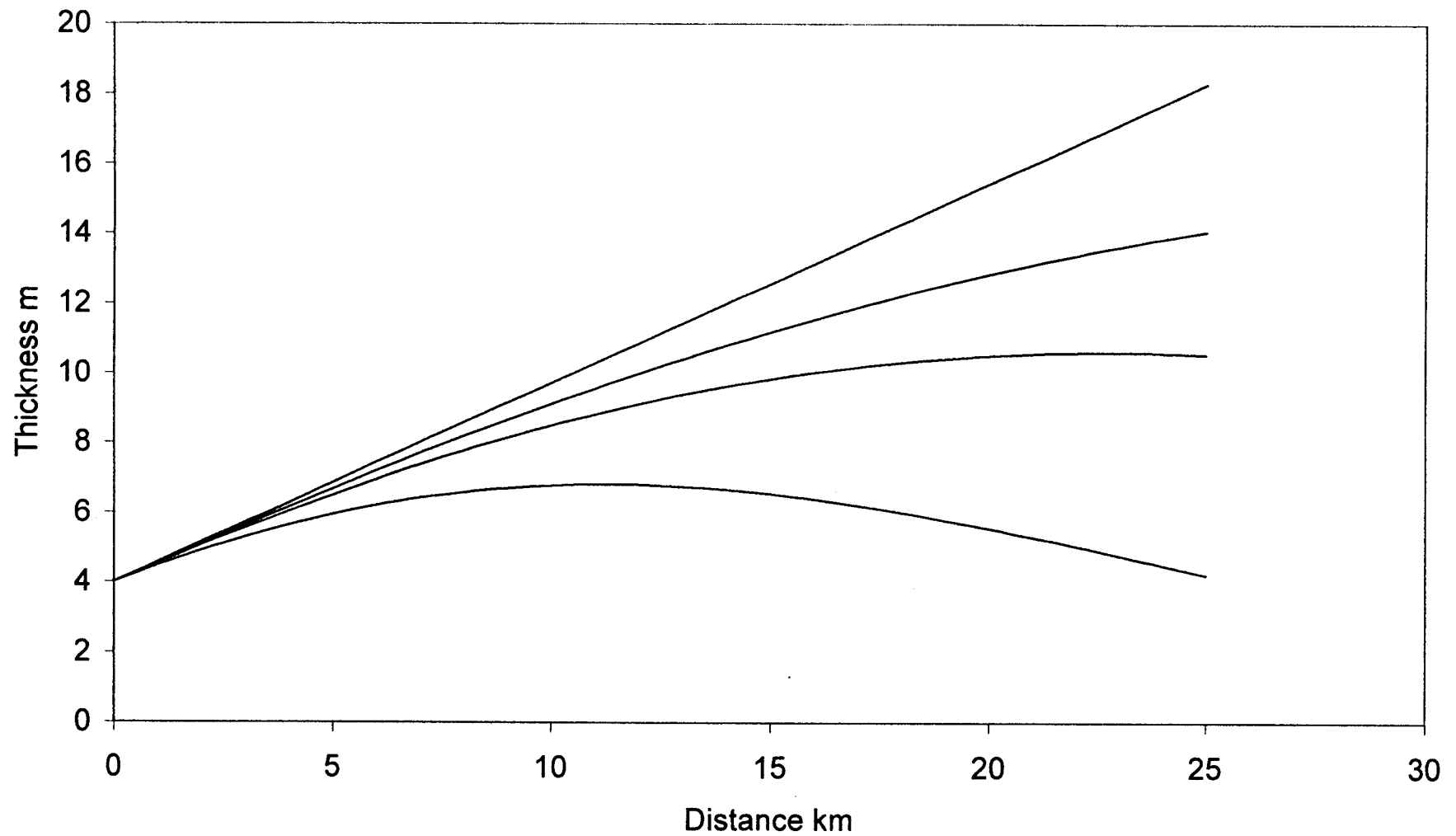


Figure 8: Flow Front Location

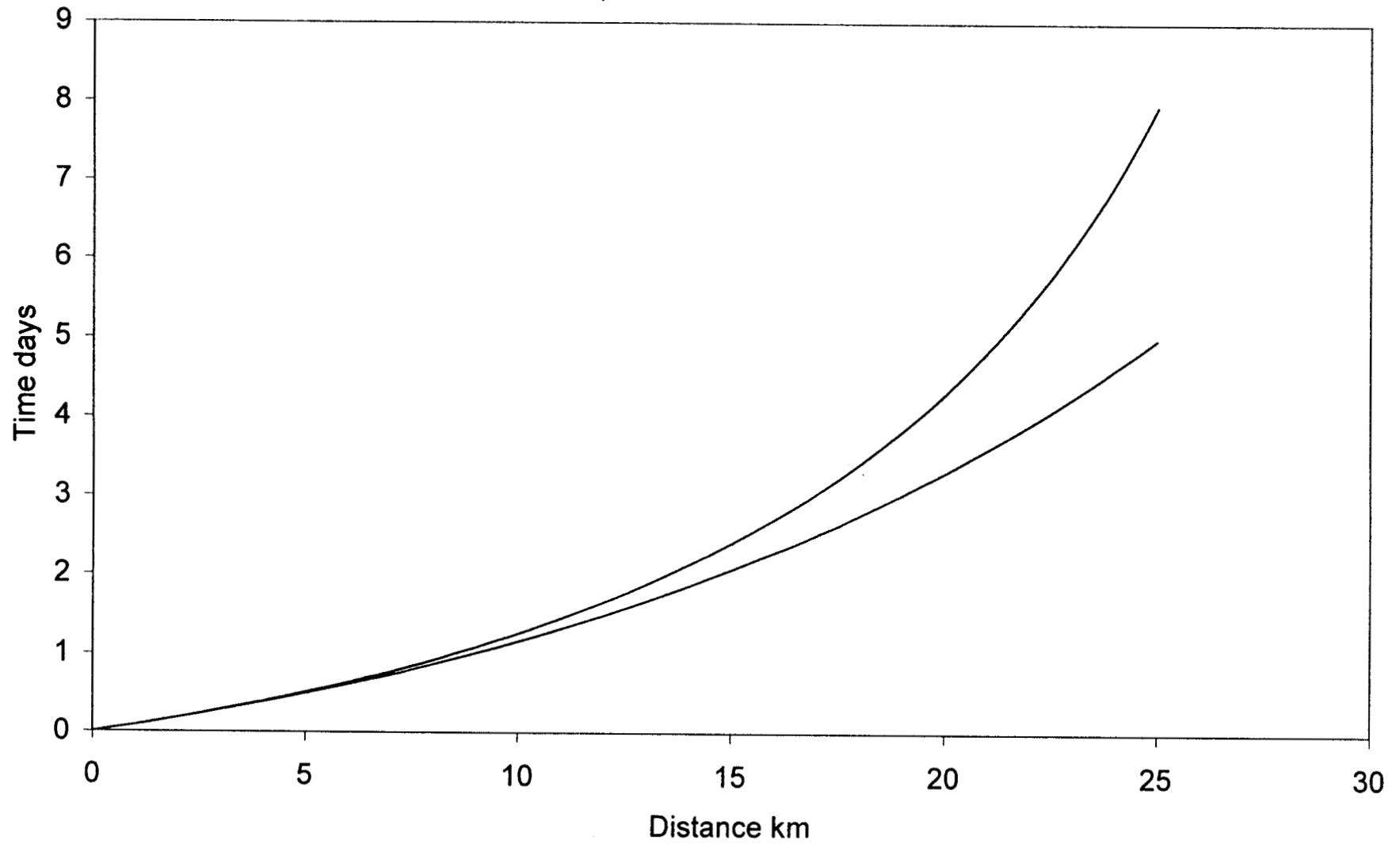


FIGURE 7 Flow thickness: Newt Q, h-dep degassing, Exp visc increase

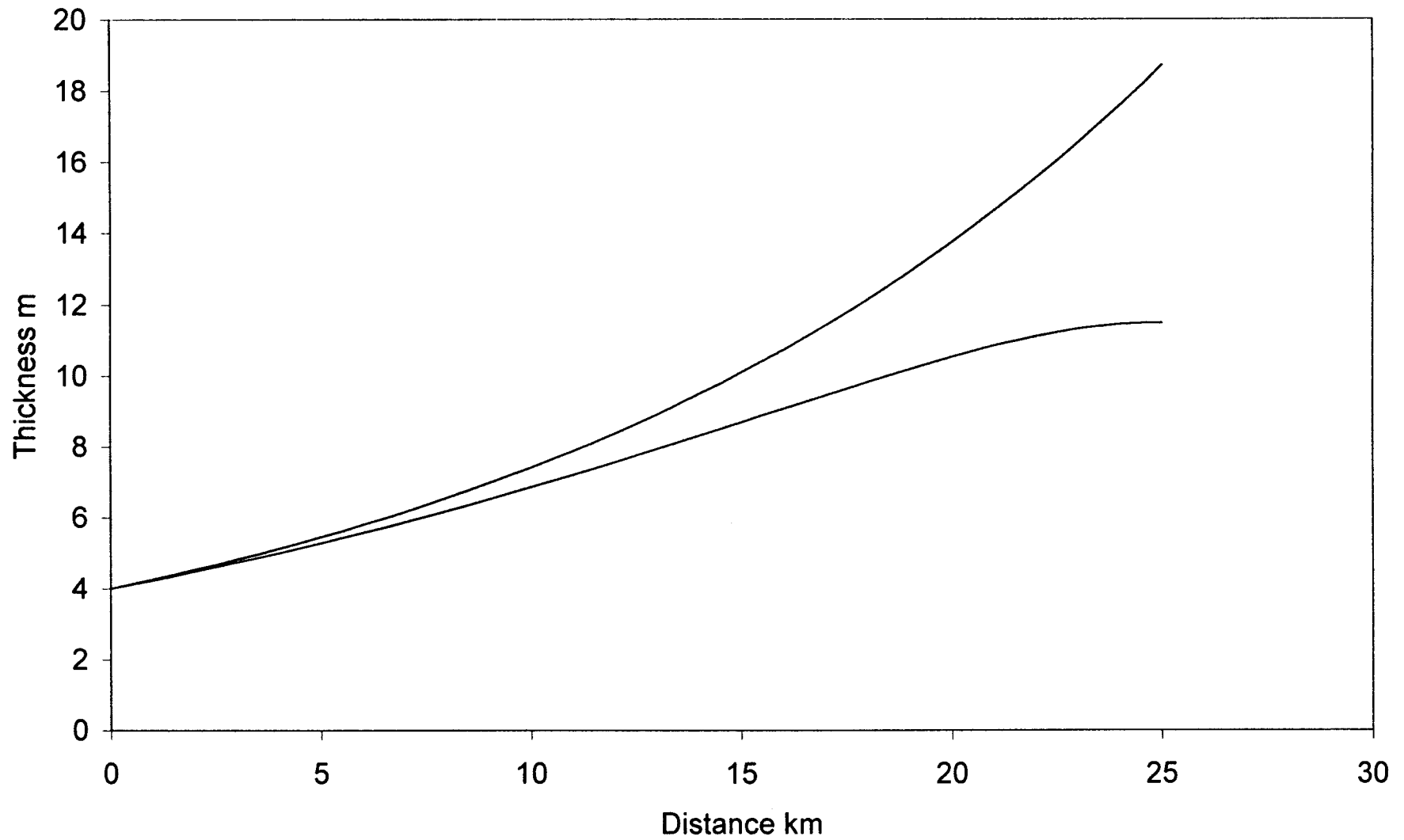


FIGURE 9: Flow thickness

